

OCNet: Object Context Network for Scene Parsing

Yuhui Yuan Jingdong Wang
Microsoft Research
{yuyua,jingdw}@microsoft.com

Abstract

Context is essential for various computer vision tasks. The state-of-the-art scene parsing methods have exploited the effectiveness of the context defined over image-level. Such context carries the mixture of objects belonging to different categories.

According to that the label of each pixel P is defined as the category of the object it belongs to, we propose the pixel-wise Object Context that consists of the objects belonging to the same category with pixel P . The representation of pixel P 's object context is the aggregation of all the features that belong to the pixels sharing the same category with P . Since the ground truth objects that the pixel P belonging to is unavailable, we employ the self-attention method to approximate the objects by learning a pixel-wise similarity map.

We further propose the Pyramid Object Context and Atrous Spatial Pyramid Object Context to capture context of multiple scales. Based on the object context, we introduce the OCNet and show that OCNet achieves state-of-the-art performance on both Cityscapes benchmark and ADE20K benchmark. The code of OCNet will be made available at <https://github.com/PkuRainBow/OCNet>.

1. Introduction

Scene parsing is a fundamental topic in computer vision and is also critical for various challenging tasks such as autonomous driving and virtual reality, in which every pixel is assigned with the category of the object that it belongs to.

FCN [11] based methods have achieved promising results with powerful representations, it still suffers from the problem of limited receptive fields and short-range context information. To capture long-range context information, the recent works [10, 26, 3] propose to employ the image-level context to augment the pixel-wise representation. The representation of image-level context is computed by employing global average pooling over the whole image or multiple sub-regions of various scales, which carries the mixture of all the existing objects in the image.

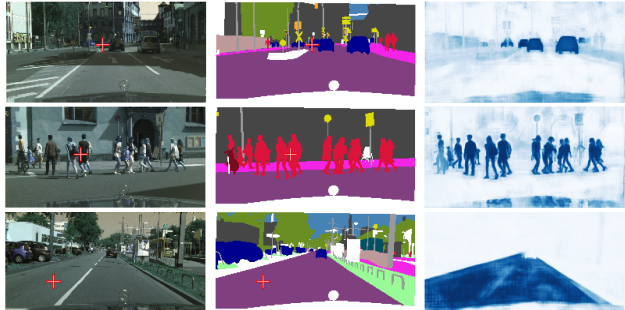


Figure 1: Pixel-wise Object Context predicted by OCNet. The first column presents three images from the validation set of Cityscapes, the second column shows their ground-truth segmentation maps and the third column illustrates the predicted attention maps with OCNet. The predicted attention map on the first row is based a pixel located in object "car", the second one is based on a pixel located in object "person" and the third one is based on a pixel located in object "road". The darkness of the color indicates the magnitude of the attention weights (the darkest blue marks the highest value).

Inspired by that the label for each pixel P is the category of the object that it belongs to, we introduce the Object¹ Context to capture the objects belonging to the same category with pixel P . Considering that the objects belonging to the same category with P are unavailable in advance, we employ the self-attention method to approximate the objects by learning a similarity map that carries the similarities between all the pixels and pixel P . We approximate the representation of the object context of each pixel P by aggregating all the features according the predicted similarity map.

We illustrate some examples of the approximated objects learned with self-attention method in Figure 1. These three images are from the validation set of Cityscapes and we choose pixels located in "car", "person" and "road" in these three images separately. The selected pixels are marked with red \oplus in both the images and the ground truth segmentation map. We illustrate the similarity maps predicted by the proposed OCNet in the third column, from which

¹Here the object includes both the things and stuff, where things are countable objects and stuff is uncountable object.

we can conclude that the predicted similarity maps well approximate both the countable objects such as "car", "person" and the uncountable object such as "road".

We further propose two kinds of extensions of the object context: Pyramid Object Context (Pyramid-OC) and Atrous Spatial Pyramid Object Context (ASP-OC). The Pyramid-OC is mainly inspired from the PSPNet and we replace all the image-level context with object context. Similarly, we also replace the image-level context within ASPP and propose the ASP-OC. Based on the object context, we propose the OCNet to capture the pixel-wise object context for each pixel adaptively.

Our main contributions are summarized as follows:

- We propose the pixel-wise Object Context to incorporate the information of objects belonging to the same category with the associated pixel P .
- The proposed OCNet achieves state-of-the-art performance on two challenging datasets including Cityscapes and ADE20K.
- All of our implementation will be open-source. We hope that OCNet provides a good baseline for the community.

2. Related Work

Semantic Segmentation. Semantic segmentation or scene parsing have achieved great progress in the recent works such as FCN [11], UNet [13], SegNet [1], ParseNet [10], PSPNet [26] and DeepLabv3 [3]. There exist two main challenges according to the recent work [3], (1) resolution: huge gap between the feature map's resolution and the input image's resolution. (e.g., the output feature map of ResNet-101 is $\frac{1}{8}$ or $\frac{1}{32}$ of the input size when we use dilated convolution [23] or not.) (2) multi-scale: there exist objects of various scales, especially in the urban scene images such as Cityscapes [4]. Most of the recent works [26, 3] are focused on methods to solve the above mentioned challenges. To handle the problem of resolution, we adopt the dilated convolution within OCNet by following the same settings in the previous works [26, 3]. Besides, it is important to capture information of multiple scales to alleviate the problem caused by multi-scale objects. PSPNet [26] applies spatial pyramid pooling while DeepLabv3 [2] employs the image-level feature augmented ASPP (atrous spatial pyramid pooling). OCNet also can capture the multi-scale context information by employing Pyramid Object Context or Atrous Spatial Pyramid Object Context.

Context. The context plays an important role in various computer vision tasks and the context can be in various

forms such as global scene context, geometric context, relative location, 3D layout and so on. Divvala *et al.* [5] used to conduct an empirical study of the influence of the context in object detection. The recent works [10, 26, 3] employ the image-level context, where the representation of the image-level context is computed by applying global average pooling over all the pixel-wise features. The image-level context considers objects of various categories while the basic goal of scene parsing is to assign the label of the objects belonging to the same category to the pixels. Thus we introduce a novel context named "object context" that carries the information of objects belonging to the same category with the associated pixel P . Especially, different pixels can access adaptive object context according to the pixel-wise similarity map learned with self-attention method. Notably, the concurrent work PSANet [27] proposes to learn the self-adaptively point-wise context by employing bi-directional information propagation. Our work is different from the PSANet from the following aspects: (1) Object context is purposed for information aggregation over the objects that the pixel P belonging to while the PSANet is proposed for information aggregation over the all the existing objects in the whole image. (2) Object context predicts the pixel-wise similarity map based on the pair-wise semantic features while the PSANet learns the pixel-wise attention map based on mainly the unary semantic features. We employ the absolute position representations [15] to study the influence of the position information while the PSANet considers the relative position information by employing over completed attention maps. (3) Object context shows significant advantages over the PSANet empirically.

Self-attention. Attention is widely used for various tasks such as machine translation, visual question answering and video classification. The self-attention [15] proposed by Vaswani *et al.* calculates the context at one position as a weighted sum of all positions in the sentence. Wang *et al.* further proposed the non-local neural network [17] for vision tasks such as video classification, object detection and instance segmentation based on the self-attention method. Our work is closely related to the self-attention and we mainly employ the self-attention method to learn the pixel-wise similarity map that used to indicate the similarities between each pixel and the associated pixel. The predicted pixel-wise similarity map is employed to approximate the objects belonging to the same category. We also extend the basic self-attention method and propose the Pyramid-OC and ASP-OC according to the challenges of scene parsing.

3. Our Approach

We introduce our approach with three subsections. First, we illustrate the formulation of the Object Context. Second, we introduce three different Object Context Modules

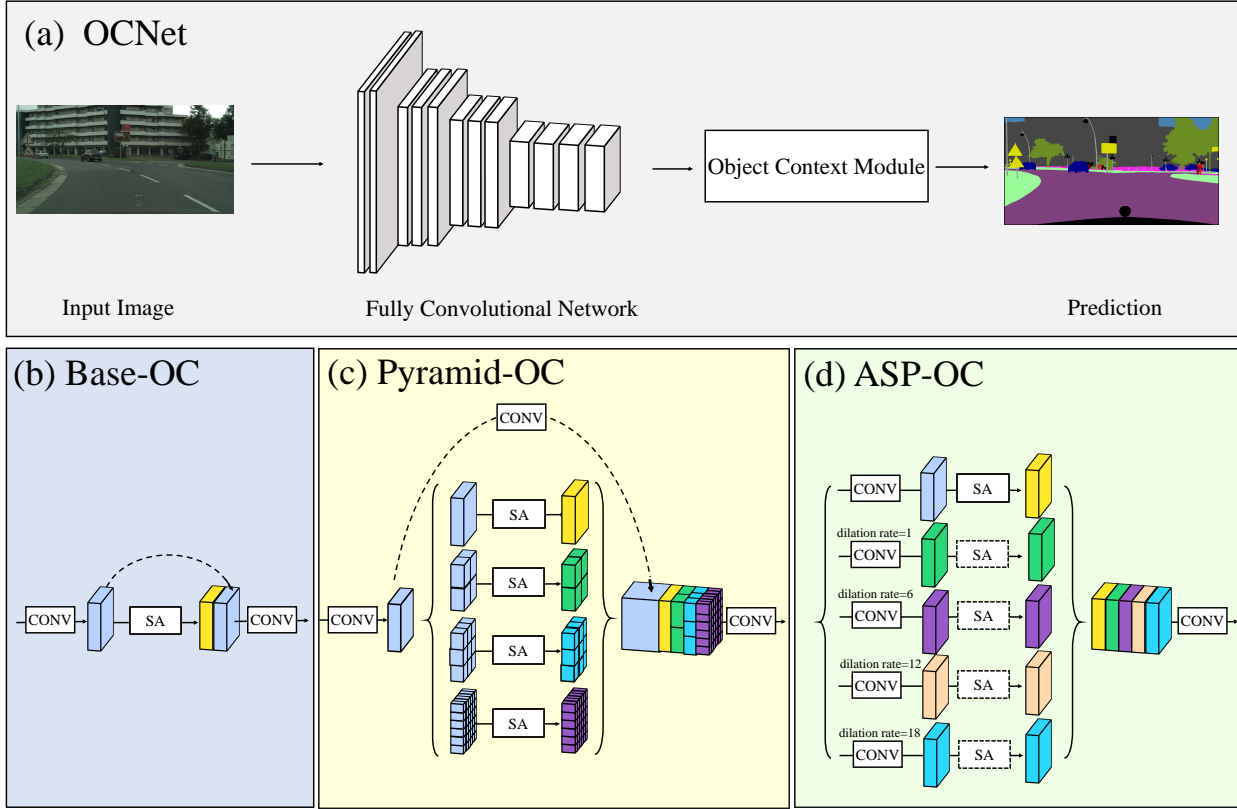


Figure 2: (a) The over-all network structure of OCNet, (b) The structure of Base-OC module, (c) The structure of Pyramid-OC module, (d) The structure of ASP-OC module (the self-attention marked with dotted line is deprecated in experiments). We approximate the pixel-wise object context with the self-attention method and we use SA to represent the self-attention method.

to compute the representations of object context including Base-OC module, Pyramid-OC module and ASP-OC module. These methods compute and employ the object context in different manners. Last, we construct the OCNet based on these Object Context Modules.

3.1. Object Context

Formulation. First, we illustrate some notations to describe our method,

- $\mathbf{X} \in \mathbb{R}^{N \times d}$: the input feature map to the object context module, where $N = H \times W$, H and W are the height and width of the feature map, d is the dimension along the channel axis. Specifically, we use $\mathbf{x}_i \in \mathbb{R}^d$ to represent the i^{th} row of \mathbf{X} .
- $\mathbf{y} \in \mathbb{R}^{N \times 1}$: the label map corresponding to \mathbf{X} , where y_i is the pixel-wise category for \mathbf{x}_i .
- $\mathbf{P} \in \mathbb{R}^{N \times d}$: the positional feature map that encodes the absolute positional information. We construct \mathbf{P} with sine and cosine functions by following

the methods proposed in self-attention [15] and image-transformer [12], where \mathbf{p}_i represents the position feature associated with \mathbf{x}_i .

- $\mathbf{C} \in \mathbb{R}^{N \times d_c}$: the representations of pixel-wise object context computed by the proposed object context module. We set $d_c = d$ for convenience and use $\mathbf{c}_i \in \mathbb{R}^d$ to record the representation of \mathbf{x}_i 's object context.
- $\mathbf{W} \in \mathbb{R}^{N \times N}$: the pixel-wise similarity map predicted by the self-attention within the object context module, where \mathbf{w}_i represents the pixel-level semantic relevance computed between the \mathbf{x}_i and \mathbf{X}_{-i} (\mathbf{X}_{-i} represents all the rows of \mathbf{X} except \mathbf{x}_i). Especially, the attention weight $w_{i,j}$ can be treated as the normalized probability of \mathbf{x}_j sharing the same category with \mathbf{x}_i and we illustrate the normalized probability in the Equation 6.

Ideally, the representation of \mathbf{x}_i 's object context can be defined as,

$$\mathbf{c}_i = \sum_{j=1}^N \mathbb{1}[y_i = y_j] \phi(\mathbf{x}_j), \quad (1)$$

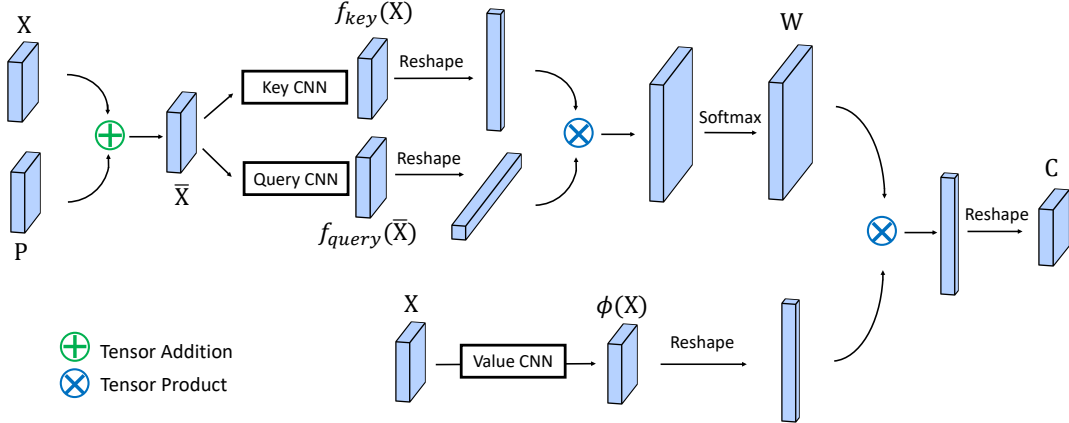


Figure 3: The Self-attention module (SA) that computes the representation of object context, there exist two branches: (1) the above branch computes the pixel-wise attention map. First, we add the position feature $\mathbf{P} \in \mathbb{R}^{H \times W \times d}$ to the semantic feature $\mathbf{X} \in \mathbb{R}^{H \times W \times d}$; then we employ the key transform and value transform to project the sum features into different embedding spaces $f_{key}(\bar{\mathbf{X}})$, $f_{query}(\bar{\mathbf{X}}) \in \mathbb{R}^{H \times W \times d}$; last, we learn the pixel-wise attention map $\mathbf{W} \in \mathbb{R}^{HW \times HW}$ in the new embedding space by applying tensor product and softmax operation. Each row of the \mathbf{W} represents the probability distribution of all the pixels that they belong to the same category with the associated pixel. (2) the under branch employs a value transform to project the feature \mathbf{X} into a different embedding space $\phi(\mathbf{X})$. Based on the pixel-wise attention map and the value embeddings, we can compute the representations of the pixel-wise object context $\mathbf{C} \in \mathbb{R}^{H \times W \times d}$.

where $\mathbb{1}[y_i = y_j]$ is an indicator function to constrain only the features of the same category with \mathbf{x}_i are considered. It is impractical to estimate the above indicator function for the testing images as we can not access the label map. So we propose to approximate the representation of \mathbf{x}_i 's object context with,

$$\mathbf{c}_i = \sum_{j=1}^N w_{i,j} \phi(\mathbf{x}_j), \quad (2)$$

where $\sum_{j=1}^N w_{i,j} = 1$ and we expect that $w_{i,j}$ should reflect the similarity between \mathbf{x}_j and \mathbf{x}_i . The distribution of weights is expected to be concentrated on the features that share the same category with \mathbf{x}_i . ϕ is used to transform the input features to a different feature space. We choose ϕ as a simple 1×1 convolution.

Self-attention. According to the methodology of self-attention, $w_{i,j}$ is defined as a function of features \mathbf{x}_i , \mathbf{x}_j , \mathbf{p}_i and \mathbf{p}_j ,

$$w_{i,j} = \Phi(\mathbf{x}_i, \mathbf{x}_j, \mathbf{p}_i, \mathbf{p}_j), \quad (3)$$

where Φ is the transform function to compute the attention weights between \mathbf{x}_i and \mathbf{x}_j . In practice, we will add the positional features \mathbf{p}_i to the semantic features \mathbf{x}_i following the self-attention. We can rewrite the above equation like,

$$\bar{\mathbf{x}}_i = \mathbf{x}_i + \mathbf{p}_i, \quad (4)$$

$$w_{i,j} = \Phi(\bar{\mathbf{x}}_i, \bar{\mathbf{x}}_j), \quad (5)$$

where the $\bar{\mathbf{x}}_i$ encodes both the semantic information and the positional information, we verify the influence of the positional features \mathbf{p}_i in our ablation study section.

Accordingly, the function Φ is defined as below,

$$w_{i,j} = \Phi(\bar{\mathbf{x}}_i, \bar{\mathbf{x}}_j) = \frac{\exp(f_{query}(\bar{\mathbf{x}}_i)^T f_{key}(\bar{\mathbf{x}}_j))}{\mathcal{C}(\bar{\mathbf{x}}_i)}, \quad (6)$$

where f_{query} is the Query transform, f_{key} is Key transform, $\mathcal{C}(\bar{\mathbf{x}}_i) = \sum_{j=1}^N \exp(f_{query}(\bar{\mathbf{x}}_i)^T f_{key}(\bar{\mathbf{x}}_j))$. We find that the choice of Key transform f_{query} and Query transform f_{key} influences the performance, thus we also conduct an ablation study in the experimental section.

The details of the self-attention are illustrated in Figure 3. Especially, the $\mathbf{X}, \mathbf{P}, \mathbf{C}$ are 2D matrixes within the formulation but are plotted with 3D tensors to ease the understanding. In fact, the conventional context can also be formulated as a special case based on Equation 2. Especially, they fix all the attention weights equally as $w_{i,j} = \frac{1}{N}$ while object context employs adaptive weights for each pixel to focus on the objects belonging to the same category with the associated pixel. Object context plays a strong counterpart for the conventional context where the object information matches the basic goal of scene parsing tasks.

3.2. Object Context Module

We mainly introduce three different object context modules to capture the object context: Base-OC, Pyramid-OC and ASP-OC.

Base-OC. First, we illustrate the design of the Base-OC module. The whole framework of Base-OC module is illus-

trated in Figure 2(b) and it mainly consists of three stages, (1) compute \mathbf{X} : a 3×3 convolution to reduce the channel dimension of the feature map from 2048 to 512, (2) compute \mathbf{C} : a self-attention module to compute the pixel-wise attention map and the representations of the object context, (more details are illustrated in Figure 3) (3) fusion: we concatenate \mathbf{C} and \mathbf{X} . The concatenated feature map will be used for further pixel-level classification. The Base-OC captures both the local context information within the \mathbf{X} and the object context information within \mathbf{C} . We further apply a 1×1 convolution to reduce the channel dimension of the fused feature maps to 512 before pixel-wise classification. Especially, there exist various choices of the first stage and we simply employ a convolution as it is not closely related to our main topic. The challenging datasets like Cityscapes and ADE20K requires context of multiple scales and we further propose the Pyramid-OC and ASP-OC.

Pyramid-OC. Inspired by the PSPNet [26], the proposed Pyramid-OC compute the object context over both the whole image and the sub-regions of multiple scales. The whole framework of Pyramid-OC is illustrated in Figure 2(c).

The Pyramid-OC is also consisted of three stages, (1) compute \mathbf{X} : a convolution to capture local context information and reduce the dimensions, (2) compute \mathbf{C} : there exist four parallel branches that capture object context of different scales. The first branch above all the other branches takes the full feature map as the input and compute the object context $\mathbf{C}_{1 \times 1}$, which is the same as the self-attention module within the Base-OC module. The second branch divides the full image map to 2×2 sub-regions equally and applies the self-attention module over each sub-region independently, where different regions share the same Key transform f_{key} and Query transform f_{query} within the second branch. Correspondingly, we get the $\mathbf{C}_{2 \times 2}$ in the second branch and $\mathbf{C}_{2 \times 2}$ is the concatenation of the representations of four object context over four sub-regions. The third branch and the fourth branch process the input feature map similar with the second branch while they divide the input to 3×3 sub-regions or 6×6 sub-regions, where we use $\mathbf{C}_{3 \times 3}$ and $\mathbf{C}_{6 \times 6}$ to record the representations of the object context computed within each divided sub-region. The Key transform f_{query} and Query transform f_{key} are not shared cross different branches. (3) fusion: first, we concatenate all the representations of the object context including $\mathbf{C}_{1 \times 1}$, $\mathbf{C}_{2 \times 2}$, $\mathbf{C}_{3 \times 3}$ and $\mathbf{C}_{6 \times 6}$ and record the concatenated representation as \mathbf{C} . then we apply a 1×1 convolution to increase the dimension of \mathbf{X} to be equal to the dimension of the concatenated representations of object context and use $\bar{\mathbf{X}}$ to represent the feature after increasing the dimensions. Third, we apply a 1×1 convolution to reduce the channel dimension of the final concatenated feature maps to 512 before pixel-wise classification.

ASP-OC. The ASP-OC module is inspired from the atrous spatial pyramid pooling (ASPP) proposed in DeepLabv3 [3]. We compute the object context over input features that capture information of different receptive fields. The whole framework of ASP-OC module is illustrated in Figure 2(d).

Specifically, the ASP-OC is consisted of three stages, (1) compute \mathbf{X} : the five branches apply different convolutions on the input feature map, where the first branch applies a convolution of 3×3 kernel size, the second branch applies a convolution of 1×1 kernel size, the third branch applies a convolution of 3×3 kernel size and dilation rate of 12, the fourth branch applies a convolution of 3×3 kernel size and dilation rate of 24, the last branch applies a convolution of 3×3 kernel size and dilation rate of 36. (2) compute \mathbf{C} : We employ the self-attention module on each branch to compute multiple representations of the object context independently. We find that the self-attention module in the second, third, fourth and last branch harms the performance in our experiments, thus we mark these self-attention modules with dotted line. (3) fusion: We concatenate the feature maps from these five branches directly and apply a 1×1 convolution to reduce the channel dimension of the concatenated feature maps to 512. The ASP-OC is employed to capture multi-scale context information, which achieves competitive performance on both datasets.

3.3. OCNet

The overall framework of OCNet is illustrated in Figure 2(a). OCNet employs a fully convolutional network to extract the feature map, an object context module to compute the pixel-wise object context and a 1×1 convolution based classifier to predict the segmentation map. We choose the ResNet-101 as the network backbone. Considering that the resolution of the predicted logits map is only $\frac{1}{8}$ of the input resolution, we apply a bilinear up-sampling to recover a prediction map of the same resolution as the input image. More implementation details are illustrated in the following sections.

4. Experiments

First, we illustrate the datasets that we use to evaluate our method. Second, we highlight all the implementation details for training the OCNet on both datasets. Then we conduct several ablation studies to investigate various factors within OCNet on Cityscapes dataset, baseline experiments on both datasets, comparison with the state-of-the-art methods on both datasets. Especially, most of our baseline experiments are re-run for three times and we report the mean and the variance to ensure that our results are reliable. Finally, we explain that the OCNet can learn meaningful object context by visualizing the pixel-wise attention maps on pixels of various categories.

4.1. Datasets

We empirically verify OCNet on two challenging datasets including Cityscapes and ADE20K. We adopt Mean IoU (mean of class-wise intersection over union) for both datasets. We need to parse both things (countable objects) and stuff (uncountable object) on the two datasets.

- **Cityscapes** is tasked for urban scene understanding, which contains 30 classes and only 19 classes of them are used for scene parsing evaluation. The dataset contains 5,000 high quality pixel-level finely annotated images and 20,000 coarsely annotated images. The finely annotated 5,000 images are divided into 2,975/500/1,525 images for training, validation and testing.
- **ADE20K** is used in ImageNet scene parsing challenge 2016, which contains 150 classes and diverse scenes with 1,038 image-level labels. The dataset is divided into 20K/2K/3K images for training, validation and testing.

4.2. Implementation Details

Network Structure Our work is implemented with Pytorch. We choose the ImageNet pretrained ResNet-101 as our backbone and make some modifications following the previous works [26] (modify the dilation rates of dilated convolution within the last two blocks with rate=2 and rate=4). The output stride becomes 8 with such modifications. We further add Base-OC block, Pyramid-OC block or ASP-OC block on the $\frac{1}{8}$ sized output feature map of ResNet-101.

Training settings For all the experiments on Cityscapes, we set the initial learning rate as 0.01 and weight decay as 0.0005 by default, the original image size is 1024×2048 and we choose crop size as 769×769 following PSPNet [26], all the baseline experiments only use the 2975 train-fine images as the training set without specification, the batch size is 8 and we choose the InPlaceABNSync [14] to synchronize the mean and standard-deviation of BN across multiple GPUs in all the experiments. We employ 40K training iterations, which takes about ~ 20 hours with $4 \times$ P100 GPUs.

For all the experiments on ADE20K, we set the initial learning rate as 0.02 and weight decay as 0.0001 by default, the input image is resized to the length randomly chosen from the set $\{300, 375, 450, 525, 600\}$ due to that the images are of various sizes on ADE20K. The batch size is 8 and we also synchronize the mean and standard-deviation of BN cross multiple GPUs. We employ 100K training iterations, which takes about ~ 30 hours with ResNet-50 and ~ 60 hours with ResNet-101 based on $4 \times$ P100 GPUs. All of our experiments on ADE20K are based on the open-source implementation [28].

Learning rate settings Similar to the previous works [3], we employ the "poly" learning rate policy on both Cityscapes and ADE20K, where the learning rate is multiplied by $(1 - \frac{\text{iter}}{\text{max-iter}})^{\text{power}}$ with $\text{power} = 0.9$.

Data augmentation For the data augmentation methods, we only apply random flipping horizontally and random scaling in the range of $[0.5, 2]$ on both datasets.

Loss function We apply basic cross entropy loss on both the final output of OCNet and the intermediate feature map output from res4b22, where the weight over the final loss is 1 and the auxiliary loss is 0.4 following the original settings proposed in PSPNet [26]. Besides, we also employ the online hard pixels mining method proposed in [18] to further improve the performance, where we only consider the loss of the hard pixels as most of the pixels can be easily discriminated. Especially, We do not apply hard pixels mining in all of our experiments unless specified to ensure the fairness of the comparison experiments.

4.3. Ablation Study

Influence of the Positional Feature. Here we study the influence of the position features. We choose the OCNet based on Base-OC block as our baseline. Base-OC (w/ P) means we consider the positional features within the self-attention module while Base-OC (w/o P) does not consider the positional information. We find that the positional information improves the mIoU on the validation set but decreases the mIoU on the test set. The related experimental results are summarized in Table 1. We disregard the positional features within the self-attention method in all of the following experiments. The possible reason for the failure of the positional features on the testing set maybe related to the choice of the positional feature, where the methodology of the position features designed for machine translation task may not suit for the scene parsing tasks.

Influence of the Key/Query transform. We use Cityscapes as our benchmark to investigate the influence of the Key/Query transform, we design five different settings based on OCNet that employs Base-OC. First, we illustrate the five different configurations of the Key/Query transform within the Base-OC module: (a) both f_{query} and f_{key} are identity transform; (b) f_{query} : 1×1 convolution, f_{key} : 1×1 convolution; (c) f_{query} and f_{key} share the same 1×1 convolution; (d) f_{query} : 1×1 convolution + BN + ReLU, f_{key} : 1×1 convolution + BN + ReLU; (e) f_{query} and f_{key} share the same 1×1 convolution + BN + ReLU. We report the related experimental results on Table 2, where each experiment is run for three times and we report the mean and the variance. We choose the choice (e) configurations for the f_{query} and f_{key} in all our latter experiments on Cityscapes. We also conduct similar study on the ADE20K dataset and set both f_{query} and f_{key} as twice of $\{1 \times 1$ convolution + BN + ReLU $\}$.

Table 1: Influence of the position features within Base-OC on Cityscapes dataset.(single crop)

Method	train mIoU(%)	val mIoU(%)	test mIoU(%)
Base-OC (w/o P)	85.21	79.19	78.07
Base-OC (w/ P)	85.22(Δ 0.01)	79.34(Δ 0.15)	77.34(Δ 0.73)

Table 2: Influence of the Key/Query transform within Base-OC on the Cityscapes dataset. (a), (b), (c), (d), (e) represent five different choices of the Key/Query transform functions.(single crop)

Key/Query choice	train mIoU(%)	val mIoU(%)
Base-OC (a)	85.17 \pm 0.01	76.42 \pm 0.19
Base-OC (b)	85.10 \pm 0.01	78.57 \pm 0.08
Base-OC (c)	85.19\pm0.01	78.64 \pm 0.06
Base-OC (d)	85.12 \pm 0.01	78.07 \pm 0.06
Base-OC (e)	85.16 \pm 0.01	78.80\pm0.07

Table 3: Influence of the Self-attention within ASP-OC. The branch column records the branches that we apply the self-attention. e.g., 1 represents that we only apply object context in the first branch.(single crop)

Method	Branch	train mIoU(%)	val mIoU(%)
ASP-OC	1	85.72\pm0.01	79.58\pm0.06
ASP-OC	1-5	81.38 \pm 0.05	75.22 \pm 0.01

Table 4: Influence of Auxiliary loss on the Cityscapes dataset. Here the experiments are based on the ResNet101-Baseline w/o object context.(single crop)

Method	Auxiliary loss	train mIoU(%)	val mIoU(%)
ResNet101	\times	84.08 \pm 0.22	74.89 \pm 0.10
ResNet101	\checkmark	84.26\pm0.23	75.69\pm0.04

Table 5: Influence of the OHEM,ms,flip, whether use validation set based on OCNet that employs ASP-OC.

OHEM	Ms,Flip	Val	mIoU(%)	test mIoU(%)
\times	\times	\times	79.58	78.22
\checkmark	\times	\times	80.41(Δ 0.83)	78.90(Δ 0.68)
\checkmark	\checkmark	\times	81.31(Δ 0.90)	80.06(Δ 1.16)
\checkmark	\checkmark	\checkmark	-	80.53(Δ 0.47)

Influence of the Self-attention in ASP-OC. We investigate the influence of the self-attention module applied on the ASP-OC module in this section. We only compare two different settings here, (1) apply self-attention on only the first branch, (2) apply self-attention on all the five branches. All the related experimental results are summarized in Table 3. Accordingly, we choose to use the first configuration.

Influence of Auxiliary loss. We add an auxiliary loss after the output of the 4th stage of ResNet to ease the optimization following the PSPNet [26]. The related comparison experiments on Cityscapes dataset are illustrated in Table 4.

Influence of the OHEM, Ms, Flip, Validation set. We adopt the online hard example mining before comparing the OCNet with the state-of-the-art methods. Following the previous works [18], the hard pixels are defined as the pixels

Table 6: Baseline Comparison experiments on Cityscapes dataset.(single crop)

Method	train mIoU(%)	val mIoU(%)
ResNet101-Baseline	84.26 \pm 0.23	75.69 \pm 0.04
ResNet101+GC	85.02 \pm 0.02	77.60 \pm 0.05
ResNet101+PSP(PSPNet)	85.26 \pm 0.01	77.84 \pm 0.19
ResNet101+ASPP(DeepLabv3)	85.64 \pm 0.01	78.65 \pm 0.03
ResNet101+Base-OC	85.16 \pm 0.01	78.80 \pm 0.07
ResNet101+Pyramid-OC	85.10 \pm 0.01	78.78 \pm 0.09
ResNet101+ASP-OC	85.72\pm0.01	79.58\pm0.06

Table 7: Baseline Comparison experiments on ADE20K.(single crop)

Method	mIoU(%)	Pixel Acc(%)
ResNet50-Baseline	34.35 \pm 0.01	76.41 \pm 0.01
ResNet50+GC	41.17 \pm 0.38	79.87 \pm 0.04
ResNet50+PSP(PSPNet)	41.34 \pm 0.01	79.96 \pm 0.01
ResNet50+ASPP(DeepLabv3)	42.53 \pm 0.03	80.44 \pm 0.01
ResNet50+OC	40.66 \pm 0.26	79.77 \pm 0.03
ResNet50+Pyramid-OC	42.28 \pm 0.08	80.21 \pm 0.03
ResNet50+ASP-OC	42.63\pm0.01	80.45\pm0.01

associated with probabilities smaller than θ over the correct classes. Besides, we need to keep at least \mathcal{K} pixels within each mini-batch when few pixels are hard pixels. e.g., we set $\theta = 0.7$ and $\mathcal{K} = 100000$ on the Cityscapes and improves 0.83 mIoU on validation set and 0.68 mIoU on test set. Then we further apply the left-right flipping and multiple scales including $[0.75 \times, 1 \times, 1.25 \times]$ to improve the performance from 80.06 to 80.53 on the test set. We can further improve the performance on test set by employing the validation set for training.

4.4. Comparison with Baseline

To evaluate the effectiveness of OCNet, we conduct a set of baseline experiments on Cityscapes and ADE20K. We use the "+GC" to represent employing the conventional global context, ResNet101+PSP represents the PSPNet that applies global context on sub-regions of multiple scales and ResNet101+ASPP follows the DeepLabv3 that incorporates the image-level global context into the ASPP module. We compare these three methods with the object context module based methods such as Base-OC, Pyramid-OC and ASP-OC. The related experimental results on Cityscapes are reported in Table 6. We can see that the our most basic method Base-OC can beat the previous state-of-the-art methods such as PSPNet and DeepLabv3. We can further improve the performance with the ASP-OC module. For example, the ASP-OC based OCNet achieves about 79.58 on the validation set based on single crop and improves about 1 point over DeepLabv3 and 2 points over PSPNet.

Additionally, we conduct a set of baseline comparison experiments on ADE20K with ResNet50. We illustrate all the related results on Table 7 and all the results are evaluated

with single crop. We can see that both ResNet50+Pyramid-OC and ResNet50+ASP-OC achieve better performance compared with the ResNet50+OC, which verifies the effectiveness of considering the multi-scale context information.

4.5. Comparison with State-of-the-art

We compare the OCNet with the current state-of-the-art methods on both datasets in this section. First, we illustrate the results on Cityscapes in Table 8 and we can see that our method achieves better performance over all the previous methods based on ResNet-101. OCNet without using the validation set achieves even better performance than most methods that employ the validation set. Especially, we adopt the strategy proposed by DeepLabV3 [3] and DenseASPP [20] to finetune the previous model(mIoU=80.53) with the fine-labeled dataset for extra epochs to further achieve better performance mIoU=81.2 with only fine-labeled dataset.

Additionally, we also compare the OCNet with the state-of-the-art methods on the ADE20K dataset and report the results in Table 9. The OCNet improves about 0.4 points over the previous state-of-the-art methods due to that the ADE20K is very challenging. We do not employ hard example mining or finetuning strategy on ADE20K dataset, which can further improve the reported performance. One observation is that the improvement on the ADE20K is not as competitive as on the Cityscapes. The main reason might be that it is hard to estimate the pixel-wise similarity map \mathbf{W} on ADE20K due to the very poor pixel-wise classification baseline.

4.6. Visualization of the object context

To verify whether the OCNet learns meaningful object context, we randomly choose some test images from the validation set of Cityscapes and visualize the pixel-wise attention map learned with OCNet based on Base-OC in Figure 4, where each attention map corresponds to the point marked with red \oplus in the left ground-truth map. These attention maps and their ground-truth maps are organized according to the category of the point marked with red \oplus .

As illustrated in Figure 4, we can find that the pixel-wise global attention maps for most classes are meaningful and capture the object context that mainly consists of pixels of the same categories. Especially, we can find that the attention map corresponding to the point on the car is mainly distributed on the pixels that construct the object cars and thus the object car's context can help the pixel-wise classification more directly compared with the image-level global context. There also exist some cases that are not satisfying such as the pixel-wise attention maps of pixels of category wall, fence and traffic sign. It is still challenging to learn better object context for pixels of the confusing categories such as traffic sign, fence, wall and so on.

Table 8: State-of-the-art Comparison experiments on Cityscapes test dataset

Method	Conference	Backbone	mIoU(%)
PSPNet [26] [†]	CVPR2017	ResNet-101	78.4
PSANet [27] [†]	ECCV2018	ResNet-101	<u>78.6</u>
OCNet [†]	-	ResNet-101	80.1
RefineNet [9] [‡]	CVPR2017	ResNet-101	73.6
SAC [25] [‡]	ICCV2017	ResNet-101	78.1
DUC-HDC [16] [‡]	WACV2018	ResNet-101	77.6
AAF [6] [‡]	ECCV2018	ResNet-101	79.1
BiSeNet [21] [‡]	ECCV2018	ResNet-101	78.9
PSANet [27] [‡]	ECCV2018	ResNet-101	80.1
DFN [22] [‡]	CVPR2018	ResNet-101	79.3
DSSPN [8] [‡]	CVPR2018	ResNet-101	77.8
DepthSeg [7] [‡]	CVPR2018	ResNet-101	78.2
DenseASPP [20] [‡]	CVPR2018	DenseNet-161	<u>80.6</u>
OCNet [‡]	-	ResNet-101	81.2

[†] train with only the train-fine datasets.

[‡] train with both the train-fine and val-fine datasets.

Table 9: State-of-the-art Comparison experiments on ADE20K validation dataset

Method	Conference	Backbone	mIoU(%)
RefineNet [9]	CVPR2017	ResNet-101	40.20
RefineNet [9]	CVPR2017	ResNet-152	40.70
PSPNet [26]	CVPR2017	ResNet-101	43.29
SAC [25]	ICCV2017	ResNet-101	44.30
PSANet [27]	ECCV2018	ResNet-101	43.77
UperNet [19]	ECCV2018	ResNet-101	42.66
DSSPN [8]	CVPR2018	ResNet-101	43.68
EncNet [24]	CVPR2018	ResNet-101	<u>44.65</u>
OCNet	-	ResNet-101	45.08

5. Conclusions

We have presented the object context that captures the information of objects belonging to the same category with the associated pixel P , which matches the basic goal of scene parsing. To approximate the unavailable objects, we employ the self-attention method to learn the pixel-wise similarity maps and verify that the predicted similarity maps can well approximate the objects. Extensive experiments on both Cityscapes and ADE20K demonstrate the advantages of object context over the conventional context. Especially, OCNet achieves stage-of-the-art performance on both Cityscapes benchmark and ADE20K benchmark.

Acknowledgments We would like to acknowledge the PSPNet baseline implemented by Zilong Huang, the valuable discussions with Kuiyuan Yang and Yuwang Wang about the importance of the object context and the design of the OCNet.

References

- [1] V. Badrinarayanan, A. Kendall, and R. Cipolla. Segnet: A deep convolutional encoder-decoder architecture for image segmentation. *arXiv preprint arXiv:1511.00561*, 2015.

[2] L.-C. Chen, G. Papandreou, I. Kokkinos, K. Murphy, and A. L. Yuille. Deeplab: Semantic image segmentation with deep convolutional nets, atrous convolution, and fully connected crfs. *IEEE transactions on pattern analysis and machine intelligence*, 40(4):834–848, 2018.

[3] L.-C. Chen, G. Papandreou, F. Schroff, and H. Adam. Rethinking atrous convolution for semantic image segmentation. *arXiv preprint arXiv:1706.05587*, 2017.

[4] M. Cordts, M. Omran, S. Ramos, T. Rehfeld, M. Enzweiler, R. Benenson, U. Franke, S. Roth, and B. Schiele. The cityscapes dataset for semantic urban scene understanding. In *Proceedings of the IEEE conference on computer vision and pattern recognition*, pages 3213–3223, 2016.

[5] S. K. Divvala, D. Hoiem, J. H. Hays, A. A. Efros, and M. Hebert. An empirical study of context in object detection. In *Computer Vision and Pattern Recognition, 2009. CVPR 2009. IEEE Conference on*, pages 1271–1278. IEEE, 2009.

[6] T.-W. Ke, J.-J. Hwang, Z. Liu, and S. X. Yu. Adaptive affinity fields for semantic segmentation. In *European Conference on Computer Vision (ECCV)*, September 2018.

[7] S. Kong and C. C. Fowlkes. Recurrent scene parsing with perspective understanding in the loop. In *The IEEE Conference on Computer Vision and Pattern Recognition (CVPR)*, June 2018.

[8] X. Liang, H. Zhou, and E. Xing. Dynamic-structured semantic propagation network. In *The IEEE Conference on Computer Vision and Pattern Recognition (CVPR)*, June 2018.

[9] G. Lin, A. Milan, C. Shen, and I. D. Reid. Refinenet: Multi-path refinement networks for high-resolution semantic segmentation. In *Cvpr*, volume 1, page 5, 2017.

[10] W. Liu, A. Rabinovich, and A. C. Berg. Parsenet: Looking wider to see better. *arXiv preprint arXiv:1506.04579*, 2015.

[11] J. Long, E. Shelhamer, and T. Darrell. Fully convolutional networks for semantic segmentation. In *Proceedings of the IEEE conference on computer vision and pattern recognition*, pages 3431–3440, 2015.

[12] N. Parmar, A. Vaswani, J. Uszkoreit, L. Kaiser, N. Shazeer, and A. Ku. Image transformer. *arXiv preprint arXiv:1802.05751*, 2018.

[13] O. Ronneberger, P. Fischer, and T. Brox. U-net: Convolutional networks for biomedical image segmentation. In *International Conference on Medical image computing and computer-assisted intervention*, pages 234–241. Springer, 2015.

[14] S. Rota Bul, L. Porzi, and P. Kotschieder. In-place activated batchnorm for memory-optimized training of dnns. In *The IEEE Conference on Computer Vision and Pattern Recognition (CVPR)*, June 2018.

[15] A. Vaswani, N. Shazeer, N. Parmar, J. Uszkoreit, L. Jones, A. N. Gomez, L. Kaiser, and I. Polosukhin. Attention is all you need. In *Advances in Neural Information Processing Systems*, pages 5998–6008, 2017.

[16] P. Wang, P. Chen, Y. Yuan, D. Liu, Z. Huang, X. Hou, and G. Cottrell. Understanding convolution for semantic segmentation. *arXiv preprint arXiv:1702.08502*, 2017.

[17] X. Wang, R. Girshick, A. Gupta, and K. He. Non-local neural networks. In *The IEEE Conference on Computer Vision and Pattern Recognition (CVPR)*, 2018.

[18] Z. Wu, C. Shen, and A. v. d. Hengel. High-performance semantic segmentation using very deep fully convolutional networks. *arXiv preprint arXiv:1604.04339*, 2016.

[19] T. Xiao, Y. Liu, B. Zhou, Y. Jiang, and J. Sun. Unified perceptual parsing for scene understanding. *arXiv preprint*, 2018.

[20] M. Yang, K. Yu, C. Zhang, Z. Li, and K. Yang. Denseaspp for semantic segmentation in street scenes. In *The IEEE Conference on Computer Vision and Pattern Recognition (CVPR)*, June 2018.

[21] C. Yu, J. Wang, C. Peng, C. Gao, G. Yu, and N. Sang. Bisenet: Bilateral segmentation network for real-time semantic segmentation. *arXiv preprint arXiv:1808.00897*, 2018.

[22] C. Yu, J. Wang, C. Peng, C. Gao, G. Yu, and N. Sang. Learning a discriminative feature network for semantic segmentation. In *The IEEE Conference on Computer Vision and Pattern Recognition (CVPR)*, June 2018.

[23] F. Yu and V. Koltun. Multi-scale context aggregation by dilated convolutions. *arXiv preprint arXiv:1511.07122*, 2015.

[24] H. Zhang, K. Dana, J. Shi, Z. Zhang, X. Wang, A. Tyagi, and A. Agrawal. Context encoding for semantic segmentation. In *The IEEE Conference on Computer Vision and Pattern Recognition (CVPR)*, June 2018.

[25] R. Zhang, S. Tang, Y. Zhang, J. Li, and S. Yan. Scale-adaptive convolutions for scene parsing. In *The IEEE International Conference on Computer Vision (ICCV)*, Oct 2017.

[26] H. Zhao, J. Shi, X. Qi, X. Wang, and J. Jia. Pyramid scene parsing network. In *IEEE Conf. on Computer Vision and Pattern Recognition (CVPR)*, pages 2881–2890, 2017.

[27] H. Zhao, Z. Yi, L. Shu, S. Jianping, C. C. Loy, L. Duhua, and J. Jia. Psanet: Point-wise spatial attention network for scene parsing. *ECCV*, 2018.

[28] B. Zhou, H. Zhao, X. Puig, S. Fidler, A. Barriuso, and A. Torralba. Scene parsing through ade20k dataset. In *Proceedings of the IEEE Conference on Computer Vision and Pattern Recognition*, 2017.

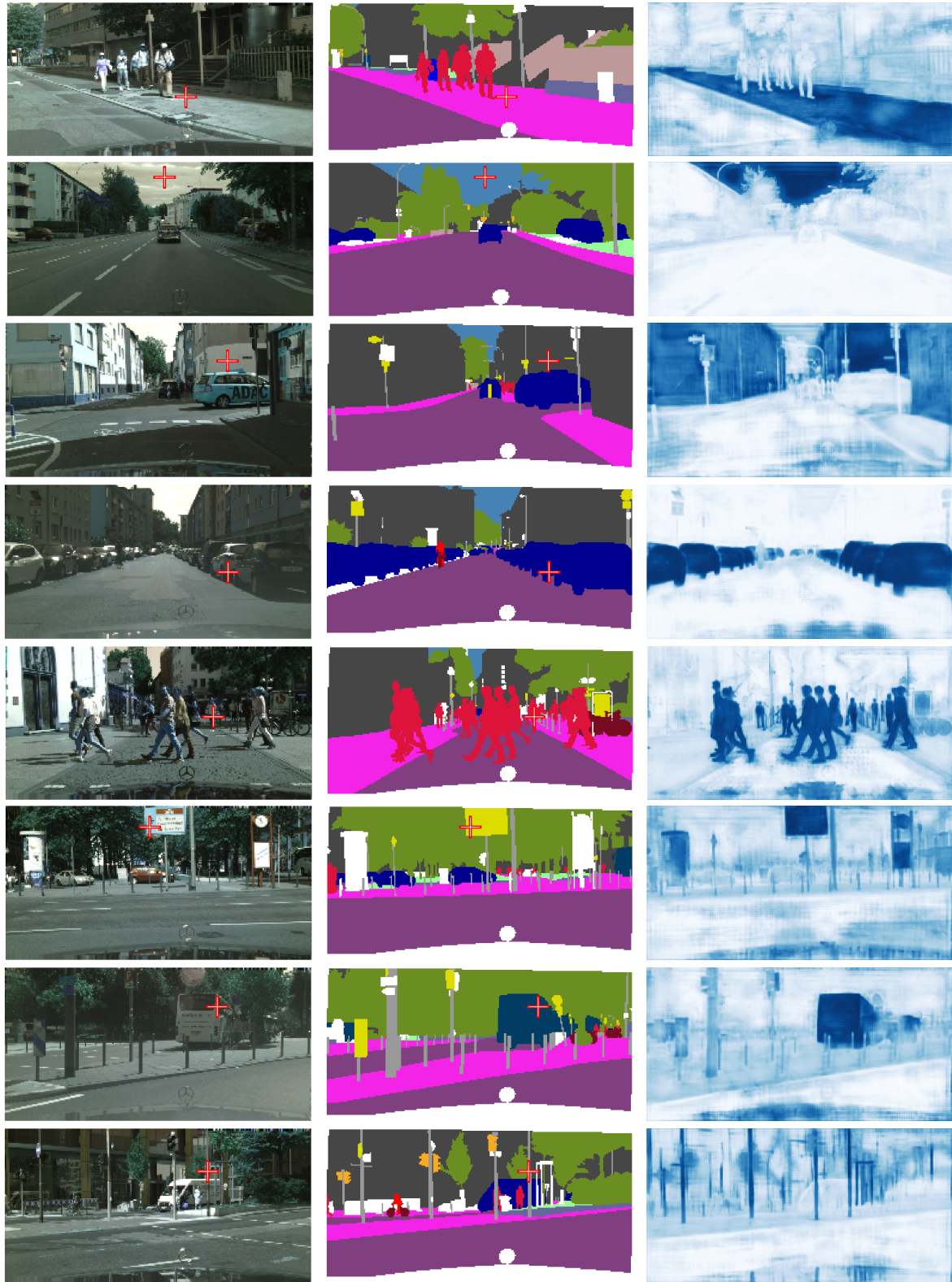


Figure 4: Visualization of pixel-wise similarity map on pixels from various categories. The left column is the images from the validation set of Cityscapes, the color map is the ground truth segmentation map while the blue map corresponds to the pixel-wise attention map, where the deeper of the blue color corresponds to the larger value of the weight. (Best viewed in color).